The effect of chordwise flexibility on the thrust and efficiency of a flapping foil

P. Prempraneerach, F.S. Hover and M.S. Triantafyllou
Department of Ocean Engineering
Massachusetts Institute of Technology
Cambridge, MA 02139
Email: pradya@mit.edu

***Abstract*— We show experimentally that properly selected chord-wise flexibility can have a significant effect on the propulsive efficiency of two-dimensional flapping (heaving and pithing) foils, up to a 36% increase, compared to the efficiency of a rigid foil, with small loss in thrust. Two different foil kinematics are employed in the experiments: the first using simple harmonic heave and pitch motions; and the second using a multi-harmonic heave motion combined with a harmonic pitch motion, selected to produce a harmonic angle of attack variation. For both types of motion, chordwise flexibility improves efficiency, the Shore A60 producing the highest efficiency; the second mode of kinematics causes the thrust coefficient to increase significantly for high Strouhal numbers. A non-dimensional *flexibility parameter* is developed which provides a scaling law for the effect of flexibility.**

I. Nomenclature

- c,s = hydrofoil chord and span lengths $[m]$
- f = heave frequency $[Hz]$
- ω = oscillating frequency $[rad/s]$
- U = horizontal towing velocity $[m/s]$
- $\frac{dh}{dt}$ = heave velocity $[m/s]$
- ϕ = the angle of attack due to heave motion $[rad]$
- θ = the physical pitch angle $[rad]$
- α = the total angle of attack $[rad]$
- ψ = the phase angle by which the pitch motion leads the heave motion $[rad]$
- ν = the kinematic viscosity of water $[m^2/s]$
- ρ = the water density $[kg/m^3]$
- h_0 = heave amplitude, limited by a travel of the linear drive $[m]$
- θ_0 = pitch amplitude $[rad]$
- h_0/c = heave amplitude to chord ratio
- Re_c = Reynolds number ($\frac{Uc}{\nu}$)
- St = Strouhal number ($2h_0f/U$)
- X(t) = horizontal instantaneous force $[N]$
- Y(t) = vertical instantaneous force $[N]$
- $\tau(t)$ = instantaneous applied torque $[N \cdot m]$
- $\bar{F_x}$, $\bar{F_y}$ = average thrust and lift forces $[N]$
- P = power input to the foil $[Watt]$

$$P = \frac{1}{T}\left(\int_0^T Y(t)\frac{dh}{dt}dt + \int_0^T \tau(t)\frac{d\theta}{dt}dt \right),$$

- C_T = thrust coefficient ($C_T = 2\bar{F_x}/\rho U^2 cs$)
- C_L = lift coefficient ($C_L = 2\bar{F_y}/\rho U^2 cs$)
- η = propulsive efficiency ($\frac{\bar{F_x}U}{P}$)

II. Introduction

Many marine animals have developed an impressive ability to move efficiently underwater. The most common means of their locomotion is the use of flapping foils or oscillating tail fins. Various types of fins employed by fishes and marine mammals have been investigated, from the high aspect ratio lunate tails employed in carangiform propulsion (Lighthill, 1970), to pectoral fins (Ramamurti *et al.,* 2002) and flippers employed by coral reef fishes, turtles and penguins.

The simplest foil to consider is the two-dimensional flapping foil. They have been investigated theoretically (Lighthill, 1970; Chopra, 1976) and experimentally (Anderson *et al.,* 1998; Haugsdal, 2000; Read *et al.,* 2003; Hover *et al.,* 2003). According to Anderson (1998), a maximum propulsive efficiency could be obtained experimentally under optimal wake conditions, forming a reverse Kármán street. Experimental results of the rigid foil with aspect ratio of 6 (Read *et al.,* 2003) exhibited an efficiency plateau of about 50-60%. Four different angle of attack profiles were systematically employed: simple harmonic motion; square; saw-tooth; and cosine angle of attack (Haugsdal, 2000). The cosine angle of attack profile, which will be called here harmonic angle of attack profile, resulted in the highest efficiency of 64%.

Large-amplitude lateral movement of the fish's flexible body, becoming maximum near the flexible tail, suggests a study of chordwise flexibility of the thrust and propulsive efficiency of a flapping foil. First, a simple harmonic motion of a two-dimensional flexible plate was analyzed using the linear theory (Wu, 1971). Inviscid theory with large amplitude oscillation (Katz, 1978 & 1979; Bose, 1995) predicted that two and three dimensional foils with chordwise flexibility perform more efficient than rigid foils, up to 20% more efficiently, with small reduction in propulsive thrust. A partially flexible foil was also shown to be more efficient than a rigid one, using a nonlinear theory employing a surface singularity distribution method with vortex-wake deformation (Kubota, 1984). Within this theory, optimal conditions are achieved when the foil flexes such that the fluid becomes more aligned with the direction of advance. Another study considered the three-dimensional oscillation of whale-fluke-shaped foil with

spanwise flexibility and aspect ratio about 6; the numerical method used a time-domain panel method (Liu *et al.,* 1997). Under proper spanwise deflection, thrust and efficiency of this passive flexible foil can be larger than for an equivalent rigid foil. Experimentally, certain types of sway and yaw motions with proper flexibility (Yamamoto *et al.,* 2001), were shown to have efficiency, an increase of up to 27%. For a two-dimensional foil, two different chordwise flexibilities were tested for certain parametric range (Castelo, 2002) and the thrust and efficiency of one of the flexible foil was found to be up to 10% and 30% higher, respectively, than those of the rigid foil.

A comparison of the propulsive efficiency of flexible foils and propellers has been conducted analytically and experimentally. Both linear and nonlinear theories with viscous and three-dimensional correction (Yamaguchi *et al.,* 1994) predicted that the efficiency of the rear-half flexible foil was 5% higher than a conventional screw propeller over a wide range of ship speed. A rectangular oscillating foil of aspect ratio 4 connected through a flexible bar was modelled as a flexible fin propeller (Lai *et al.,* 1989). An experimental propulsive efficiency of around 0.7 was reported, which was in agreement with linear unsteady-flow model prediction.

In this paper, we investigate the propulsive thrust and efficiency for five different chordwise-flexible foils, as well as for a rigid foil. We employ two different kinematic patterns, the first consisting of simple harmonic heave and pitch motions; and the second consisting of heave and pitch motions producing a simple harmonic angle of attack variation. The Shore A60 foil performs best, with maximum propulsive efficiency of 87%, about 36% higher than that of a rigid foil, at a maximum angle of attack of 15°. Comparison of the flexible-foil results versus the results from conventional propellers (Breslin *et al.,* 1994), viz. the Kirsten-Boeing propeller, a contrarotating propeller, as well as the theoretical propeller performance predicted by lift-line theory, show that the flexible foil outperforms these conventional propeller over certain parametric ranges.

III. Experimental Setup and Procedure

All tests were conducted at the Ocean Engineering Testing Tank. The working dimensions of the tank are: 17 m long x 2.44 m wide x 1.52 m deep. A tow-rail carriage system, shown in Figure 1, was used for the tests.

Each foil consists of an aluminum beam core covered with cast flexible urethane to form a NACA 0014 foil shape, having chord and span lengths of 10.0 cm and 49.4 cm, respectively. The cross-section of the structure is shown in Figure 2. Five 1 cm diameter holes are drilled in the aluminum core so that the poured urethane makes a complete bond allowing no relative rotation. Steel shafts at either end of the beam connect to streamlined aluminum struts through universal joints. The purpose of the universal joints is to accommodate misalignment between the shafts on both sides of the foil.

The lower part of the carriage, i.e., the part submerged in the water, can be oscillated in the vertical direction with a

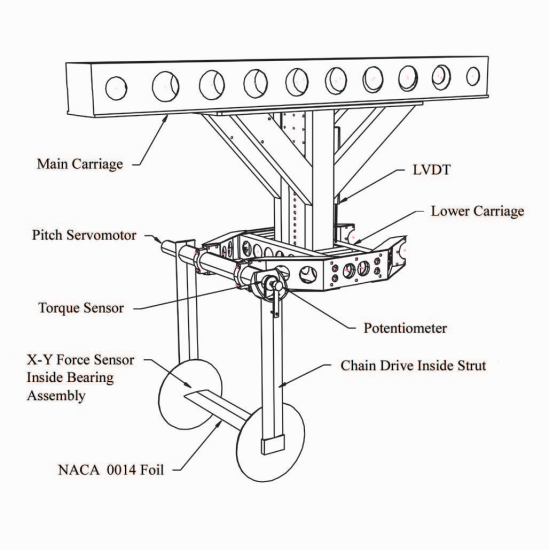

Fig. 1. View of the carriage and foil assembly.

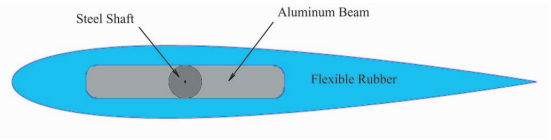

Fig. 2. The cross-section of the foil design.

specified amplitude and frequency through a liner drive, while the main carriage moves forward at constant speed. The foil-driving apparatus consists of the two aluminum struts firmly connected by an aluminum tube, attached to the lower carriage; the foil is mounted at the bottom of the struts. Acrylic circular end plates are placed at the ends of the foil to promote two-dimensional flow. On the right side strut, a KISTLER 9117 three-axis piezoelectric force sensor, measuring the horizontal (drag/thrust) and vertical (lift) forces, is connected to one of the shafts of the foil. On the left side strut, a gear is connected, driven by a chain attached to a pitch servomotor above the waterline. A KISTLER 9065 torque sensor and a potentiometer are connected to the servomotor shaft to measure the applied torque and the pitch angle correspondingly. The heave and pitch motions of the foil are controlled by a computer using a three-axis PID motion control card, and recorded along with force and torque using a DAS16/Jr card along with the DASYLab program.

Two different modes of motion were employed in the present work. In the first mode, which we call the ”simple harmonic motion” profile, sinusoidal heave and pitch trajectories are used. In the second mode, called the ”harmonic angle of attack” profile, we employ a multi-harmonic heave motion together with a harmonic pitch motion, to achieve a net sinusoidal nominal angle of attack profile. The nominal angle of attack is defined in Figure 3; here, V the resultant velocity of the foil. If the foil only heaves up and down, $\phi(t)$ is found as

$$\phi = \arctan(\dot{h}/U).$$

The total angle of attack, $\alpha(t)$, including the effects of pitching and heaving, can be computed as:

$$\alpha(t) = \phi(t) - \theta(t).$$

We define in detail the two modes of motion in the next sections. The first mode, is the simplest one, consisting of harmonic heave and pitch motion. The second one, enforces a harmonic angle of attack variation, which is especially important for high Strouhal numbers, where the first mode provides multi-harmonic angle of attack, which is accompanied by multi-vortex shedding. A harmonic angle of attack variation has been found to enhance the thrust coefficient without effect on the efficiency of the foil Read et al [17]).

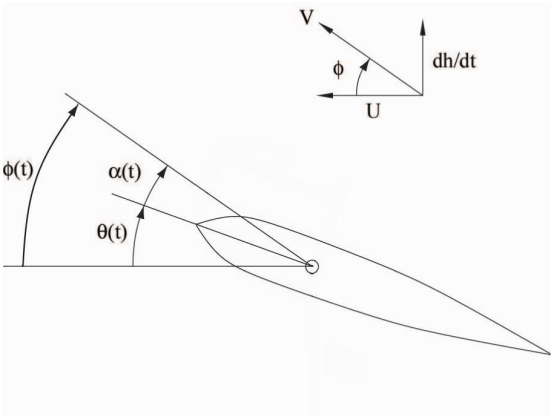

Fig. 3. Diagram of the angle of attack (Read et al 2003)

A. Simple Harmonic Motion Profile

Within this motion scheme, the heave and pitch motions are described by sinusoidal functions of time: $h(t) = h_0 \sin(\omega t)$ and $\theta(t) = \theta_0 \sin(\omega t + \psi)$. The phase angle, ψ, for all the experiments reported here was set equal to $\pi/2$. Thus, the angle of attack for this simple harmonic profile can be written as:

$$\alpha(t) = \arctan\left(\frac{h_0 \omega \cos(\omega t)}{U}\right) - \theta_0 \cos(\omega t)$$

The angle of attack profile resulting from harmonic heave and pitch has a non-sinusoidal shape due to the arc-tangent function. As discussed in Hover *et al.* (2003), for certain regimes the arctangent has a negligible effect, while for other regimes it causes significant degradation of thrust performance.

B. Harmonic Angle of Attack Profile

A combination of a multi-harmonic heave motion and simple harmonic pitch can produce a harmonic angle of attack profile, expressed as $\alpha(t) = \alpha_{max} \cos(\omega t)$. Following Hover *et. al* (2003), the heave velocity can be described by the following transposition of the above equation:

$$\dot{h}(t) = \tan(\alpha(t) + \theta_0 \cos(\omega(t) + \psi)) \cdot U.$$

Thus, the heave motion is found from this expression, while the θ_0 angle can be found iteratively to minimize $\dot{h}$, for each parametric combination.

Experiments for each foil were conducted within the range of kinematic variables shown in Table I. A heave amplitude to chord ratio h_0/c of 0.75, and a ninety-degree phase between heave and pitch (ψ), were used in all the experiments. According to Read's experiment [17], the value ψ = 90° is more robust in efficiency to a change of St number. The Strouhal number and angle of attack were investigated in 0.05 and 5-degree increments, respectively.

TABLE I

Test matrix for both α profiles.

St	$\alpha_{max}(deg)u$	Re_c
$0.1 - 0.45$	$10 - 30$	4×10^4

To illustrate the actual force produced from the rigid foil, the magnitude and direction of total instantaneous force, whose components are the lift and thrust forces, varying as the foil moves from left to right and oscillates, are shown in Figure 4 for St of 0.3 and maximum angle of attack α of 30°.

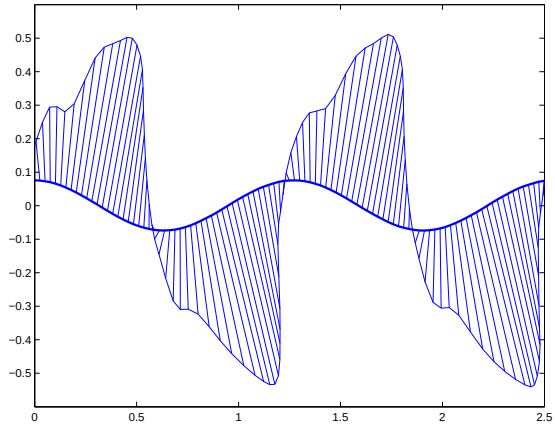

Fig. 4. Fluid force acting on the rigid foil, moving from left to right, when St = 0.3 and α 30°. The magnitude of both thrust and lift forces are scaled down with 1:1 ratio.

C. Elasticity Measurement

We measured the Young's modulus E for the various urethane rubbers we used, which are described in terms of Shore A hardness. Rectangular cross-section beams, with 2 cm width, 3 cm height and 15 cm length, were molded from urethane rubbers with the following Shore designations: A10, A30, A50, A60 and A70. We hung known weights from the middle of each simply-supported beam, and measured repeatedly the

deflection at the mid-point. The computed values of the mean E, as a function of Shore A hardness, are shown in Figure 5, and the variation in measurement is given through an error bar. Clearly, the modulus is not linearly dependent on the Shore A hardness; instead, an approximately parabolic dependence is found. The mean values are given also in Table 2.

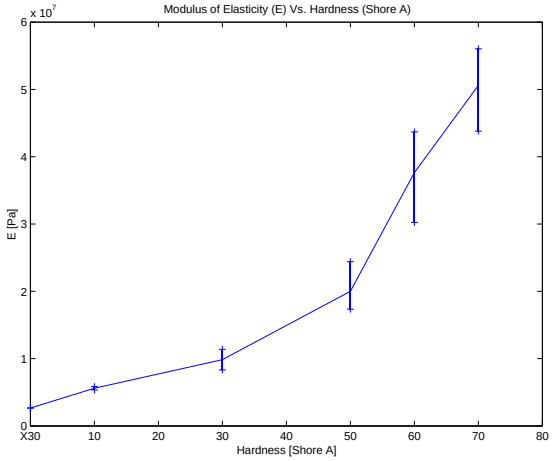

Fig. 5. The modulus of elasticity for various Shore A hardness urethane rubbers, from beam-deflection measurements.

Note that for the Shore A30 material, we used two different specimens, produced inadvertently under different circumstances: we measured a lower E, value when an older rubber mix was used. This material, which we will refer to as "X30," provides E lower than for the Shore A10 rubber.

D. Non-dimensional parameter of foil stiffness

We now develop a single non-dimensional parameter to quantify the foil stiffness in comparison to the fluid forces. We define the non-dimensional foil stiffness, $\hat{e}$, as the ratio of: the force, P, which, if distributed uniformly over the foil's upper surface, causes the trailing edge to deflect ten percent of the chord length, divided by the lift force due to fluid loading, i.e., $\hat{L} = \frac{1}{2}\rho U^2 C_L(sc)$. For the linear calculation of P, we assume the foil to be constrained in rotation at a distance $c/3$ from the leading edge. The following formula for P, derived for the NACA 0014 foil, is obtained from numerical solution of the beam equation:

$$P = 4.8 \cdot 10^{-3} E c^2$$

Then, the non-dimensional foil stiffness, $\hat{e}$, using a beam with uniform cross-section can be found as:

$$\hat{e} = \frac{F(\frac{2c}{3})}{\hat{L}} = 2.6 \cdot 10^{-4} \frac{E}{\rho U^2 C_L}.$$

Hence, $\hat{e}$, for a given foil shape, is found to be proportional to E and inversely proportional to U^2. If C_L is taken as equal to one, this non-dimensional stiffness can be used instead of E to represent the relative hardness of urethane rubber, as shown in Table II for the towing velocity of 0.3 and 0.4 m/s. The non-dimensional foil stiffness, $\hat{e}$, is provided also as a function of Shore number and Reynolds number in Figure 6.

TABLE II

The mean Young Modulus for various Shore A hardness; and the non-dimensional foil stiffness for towing velocity of 0.3 and 0.4 m/s.

$ShoreA$ $hardness$	E_{mean} $(\cdot 10^7)[Pa]$	$\hat{e}$ for $U = 0.3[m/s]$	$\hat{e}$ for $U = 0.4[m/s]$
$X30$	0.3183	9	5
$A10$	0.5596	16	9
$A30$	0.9855	28	16
$A50$	1.9996	57	32
$A60$	3.4617	99	56
$A70$	5.0591	145	81

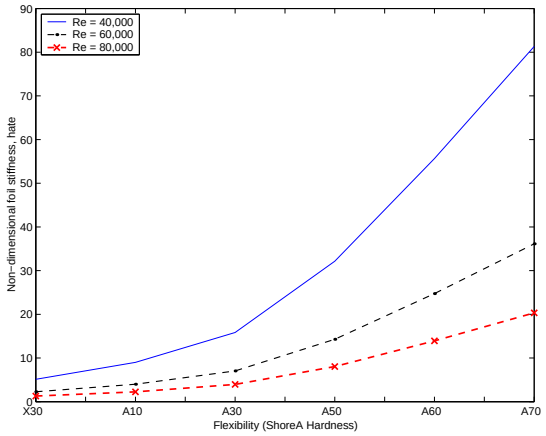

Fig. 6. The non-dimensional foil stiffness as function of Shore A flexibility and the Reynolds number.

IV. Experimental Results

Our overall findings are shown in Figures 7, where thrust performance (C_T) and efficiency (η) are given as a function of stiffness $\hat{e}$, for several Strouhal numbers. The data shown represent maximum values taken over all the angles of attack considered. With Strouhal number range between 0.1-0.45, substantial efficiency gains are seen with $\hat{e} \approx 60$; there is no significant variation of thrust performance, across the range of stiffnesses tested. These broad descriptions are true for both kinematic profiles used, i.e simple harmonic motion profile, and harmonic angle of attack profile.

A. Simple Harmonic Motion Profile

We show the mean thrust coefficient and efficiency for the Shore A60 and rigid foils in Figures 8 and 9. We found that C_T and η, for different chord-wise flexibility than Shore A60, are qualitatively similar to the results for Shore A60; hence the other cases are not shown. Error bars indicate the min-max variation resulting from at least two experimental runs for

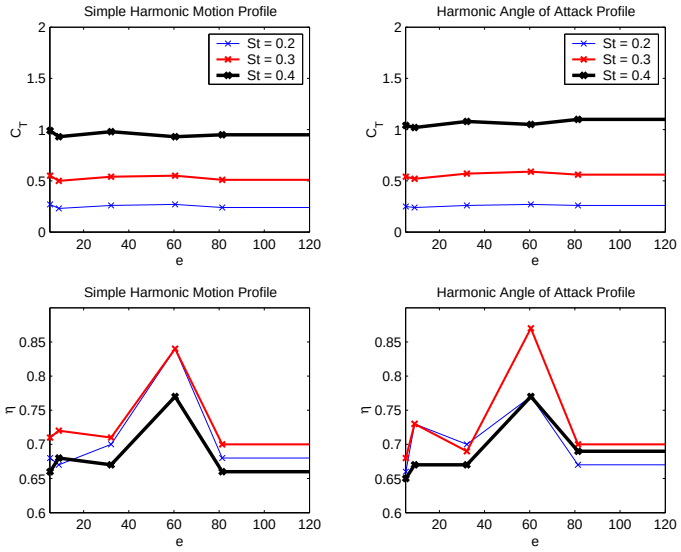

Fig. 7. The thrust coefficient (top row) and the propulsive efficiency (bottom row) as function of the non-dimensional foil stiffness using the simple harmonic motion profile (on the left) and the harmonic angle of attack profile (on the right).

each condition, obtained on different days of testing. Also, for Strouhal number 0.1 and angle of attack of $10°$, there are large variations in the experimental results, because the magnitudes of the measured horizontal and vertical forces, as well as the applied torque on the foil, are very small. Thus, although some data at this condition are shown in the plots, we do not provide detailed comparisons for that specific parametric range.

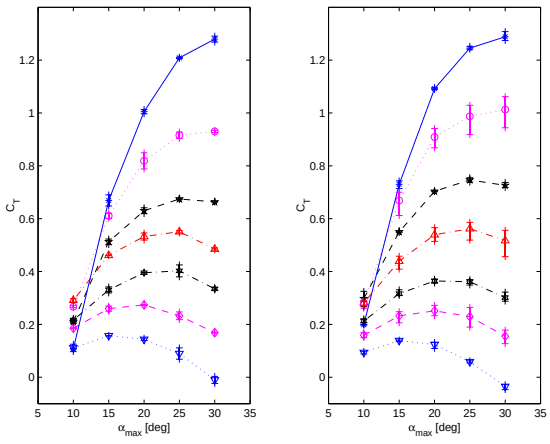

Fig. 8. The thrust coefficient for the flexible Shore A60 foil (on the left) and the rigid foil (on the right).

Table III shows the thrust and efficiency results for all the stiffnesses used. Two columns in the table provide the thrust and efficiency of the flexible foil divided by the corresponding values of the rigid foil; these are called the normalized thrust and efficiency.

The chordwise flexibility does not have a systematic effect on the thrust coefficient, for the entire St range shown. For all foils, the larger the Strouhal number is, the larger the

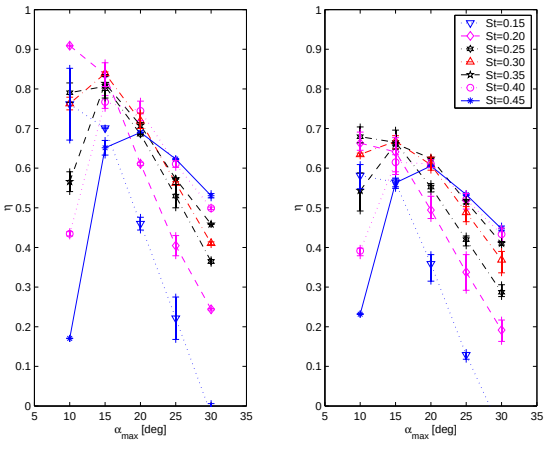

Fig. 9. The propulsive efficiency for the flexible Shore A60 foil (on the left) and the rigid foil (on the right).

thrust coefficient becomes. The variation with α_{max} is quite consistent also; for high St the thrust coefficient increases with St up to an angle of attack value of at least $30°$. For lower values of St, the thrust coefficient decreases for lower α_{max} because of the prevalence of the arctangent function in the angle of attack expression provided above. In Table 3, thrust is evidently slightly improved by flexibility for lower Strouhal numbers, but is degraded at higher St values.

Propulsive efficiency of the A60 foil is significantly higher than for all other foils, including the rigid one. This regime of enhanced efficiency is most notable at the lower angles of attack considered; but efficiency is higher than for the rigid foil for all angles of attack. At the optimum α_{max}, the A60 foil can achieve at least a twenty percent improvement in efficiency over the rigid foil, for $St \leq 0.40$. The other flexible foils achieve a five to ten percent improvement compared to the rigid foil. Propulsive efficiency for all flexible foils approaches a maximum value when the Strouhal number is between 0.2 and 0.35. This is in good agreement with the range of 0.25-0.4 posited by Triantafyllou & Triantafyllou (1993).

Contour plots of the thrust coefficient and efficiency for various chordwise flexibilities, shown in Figures 10 and 11, respectively, further exhibit the broad improvement in the propulsive efficiency due to the chordwise flexibility. The eighty percent efficiency contour of the A60 foil occurs below 15 degrees maximum angle of attack and for Strouhal numbers between 0.17 and 0.35, whereas this level is never reached for any of the other foils. The seventy percent contour has a similar character for the three softest foils (X30, A10, and A30), but expands in the A60 case to cover nearly all tested conditions with $\alpha_{max} \leq 20°$, and then shrinks and disappears as the stiffness increases further. The fifty percent efficiency contour changes very little with foil flexibility.

B. Harmonic angle of attack profile

The broad characteristics of the thrust coefficient and propulsive efficiency using the harmonic angle of attack profile are quite similar to those using the simple harmonic motion

TABLE III

The maximum values for the mean C_T and η and normalized C_T and η at different α_{max} and Strouhal number between 0.1 and 0.45 using the simple harmonic motion profile.

Flexibility	St	α_{max} *for* $C_{T_{max}}$	$C_{T_{max}}$	$C_{T_{norm}}$	α_{max} *for* η_{max}	η_{max}	η_{norm}
$ShoreX30$	0.15	15	0.16	1.14	15	0.63	1.12
$ShoreA10$		15	0.13	0.93	15	0.57	1.02
$ShoreA50$		15	0.16	1.14	15	0.68	1.20
$ShoreA60$		15	0.16	1.14	15	0.70	1.25
$ShoreA70$		15	0.13	0.93	15	0.57	1.01
$Rigid$		15	0.14	1	15	0.56	1
$ShoreX30$	0.20	20	0.27	1.08	15	0.68	1.07
$ShoreA10$		20	0.23	0.92	15	0.67	1.02
$ShoreA50$		20	0.26	1.04	15	0.70	1.09
$ShoreA60$		20	0.27	1.08	15	**0.84**	**1.31**
$ShoreA70$		20	0.24	0.96	15	0.68	1.06
$Rigid$		20	0.25	1	15	0.64	1
$ShoreX30$	0.25	20	0.41	1.14	15	0.70	1.05
$ShoreA10$		20	0.37	1.03	15	0.70	1.06
$ShoreA50$		20	0.39	1.08	15	0.68	1.03
$ShoreA60$		20	0.40	1.11	15	0.81	1.21
$ShoreA70$		20	0.37	1.07	15	0.71	1.06
$Rigid$		20	0.36	1	15	0.67	1
$ShoreX30$	0.30	25	0.55	0.98	15	0.71	1.06
$ShoreA10$		25	0.50	0.89	15	0.72	1.08
$ShoreA50$		25	0.54	0.96	15	0.71	1.06
$ShoreA60$		25	0.55	0.98	15	0.84	1.25
$ShoreA70$		25	0.51	0.91	20	0.70	1.05
$Rigid$		25	0.56	1	15	0.67	1
$ShoreX30$	0.35	25	0.76	1.01	15	0.69	1.05
$ShoreA10$		25	0.70	0.93	15	0.69	1.05
$ShoreA50$		25	0.74	0.99	15	0.70	1.05
$ShoreA60$		25	0.67	0.89	15	0.81	1.23
$ShoreA70$		30	0.72	0.96	15	0.67	1.04
$Rigid$		25	0.75	1	15	0.66	1
$ShoreX30$	0.40	30	0.99	0.98	15	0.66	1.07
$ShoreA10$		30	0.93	0.92	15	0.68	1.10
$ShoreA50$		30	0.98	0.97	15	0.67	1.09
$ShoreA60$		30	0.93	0.92	15	0.77	1.24
$ShoreA70$		30	0.95	0.94	15	0.66	1.08
$Rigid$		30	1.01	1	15	0.62	1
$ShoreX30$	0.45	30	1.29	1.00	20	0.64	1.05
$ShoreA10$		30	1.22	0.95	20	0.65	1.07
$ShoreA50$		30	1.24	0.96	20	0.62	1.03
$ShoreA60$		30	1.28	0.99	20	0.69	1.13
$ShoreA70$		30	1.27	0.98	20	0.63	1.04
$Rigid$		30	1.29	1	20	0.61	1

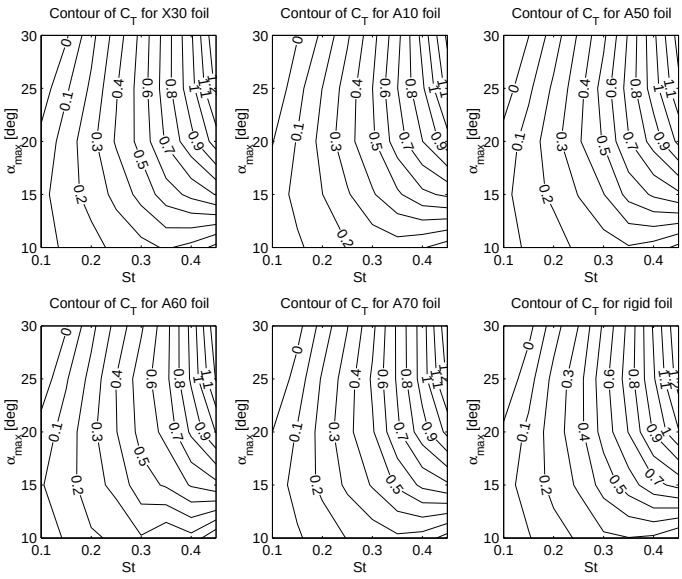

Fig. 10. The contour of the thrust coefficient for Strouhal number between 0.10-0.45

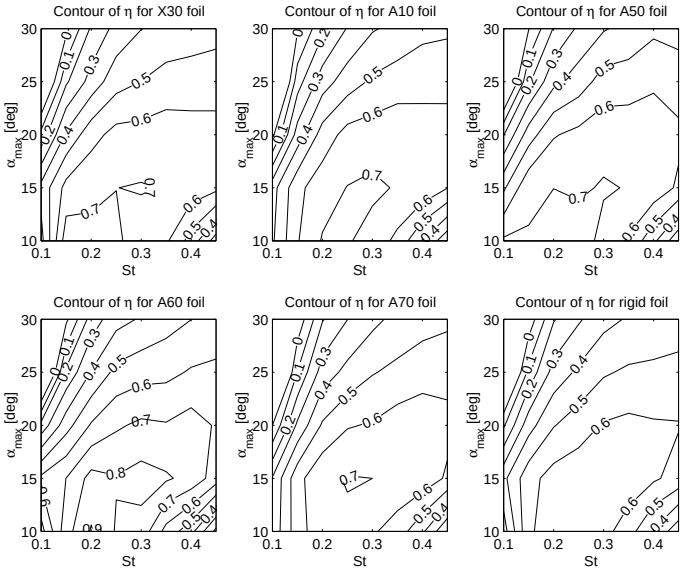

Fig. 11. The contour of the propulsive efficiency for Strouhal number between 0.10-0.45

profile. Namely, with various chordwise flexibility values, the thrust coefficient is quite comparable for all foils, while the efficiency of the Shore A60 is highest.

The thrust coefficient and efficiency plots of the Shore A60 and rigid foils are shown in Figure 12 and 13, respectively. We include curves from the case of simple harmonics, and observe that substantial gains in thrust are brought about by the angle of attack correction. For instance, at St of 0.45 and 30°, the C_T of rigid foil with harmonic angle of attack profile is greater than that with simple harmonic profile by 0.18, or 14%. The propulsive efficiencies from simple harmonic and harmonic angle of attack profiles, however, are almost identical.

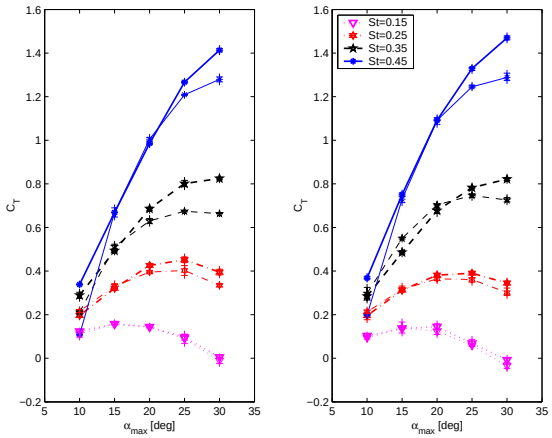

Fig. 12. The thrust coefficient for the flexible Shore A60 foil is shown on the left and the rigid foil is shown on the right (thick line: with harmonic angle of attack profile; thin line: with simple harmonic motion profile).

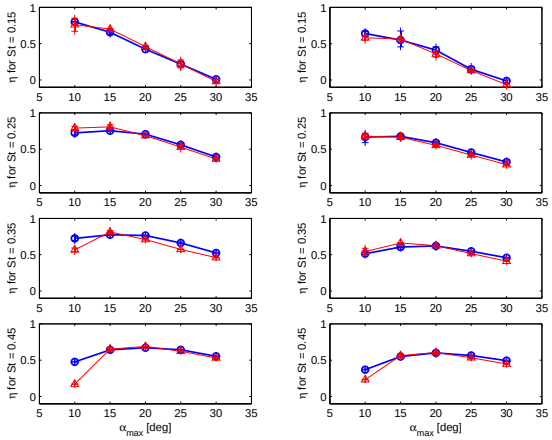

Fig. 13. The propulsive efficiency for the flexible Shore A60 foil is shown on the left and the rigid foil is shown on the right (thick line: with harmonic angle of attack profile; thin line: with simple harmonic motion profile).

Similar to the case of the simple harmonic profile, with St between 0.1 to 0.45 the Shore A60 foil yields the best efficiency among all tested foils. At St of 0.3 and 15° angle of attack, the efficiency of the A60 foil reaches a value of 0.87, which is 36 % higher than the rigid foil's efficiency; the concurrent thrust coefficient of the A60 foil is seven percent higher than the rigid foil's. The optimum efficiency of the A60 foil, using the harmonic angle of attack profile, occurs at a higher Strouhal number (0.3) than in the simple harmonic profile (0.2).

To evaluate the effect of the chordwise flexibility, C_T and η of all flexible foils is normalized with the C_T and η of the rigid foil, i.e., the $C_{T_{norm}}$ and η_{norm} defined previously. In Table IV, we see that thrust is enhanced by the flexibility - A60 in particular - for the lower range of St, but then degraded by it at the higher St.

Efficiency is similar to the simple harmonic motion case, as the A60 foil generally provides a twenty percent improvement over the rigid foil case, with the other flexible foils improving

five to ten percent. The A60 foil has a maximum efficiency at $St = 0.30$.

We define a second normalization to account for the combined effect of flexibility and the angle of attack correction, by dividing experimental results by the data from the corresponding foil under simple harmonic motion. In Table IV, these new coefficients are $\tilde{C}_{norm}$ and $\tilde{\eta}_{norm}$. First, the effect only due to harmonic angle of attack can be observed from $\tilde{C}_{T_{norm}}$ and $\tilde{\eta}_{norm}$ for the rigid foil. The angle of attack correction alone improves the thrust coefficient by about ten percent at high Strouhal number, but it does not have much influence on the efficiency for any Strouhal number. Second, the impact of the angle of attack correction on a flexible foil is assessed by comparing the two normed quantities. Below $St = 0.3$, gains in thrust due to flexibility are degraded by the harmonic angle of attack profile, but above $St = 0.3$, mild reductions in thrust due to flexibility are counteracted and improved by the harmonic angle of attack. The highest thrust coefficient is obtained at $St = 0.25$, with the A60 foil and no angle of attack correction. The effect of harmonic angle of attack on the efficiency is comparatively mild, and operation without the correction, and at $St = 0.3 - 0.35$, seems to be optimum.

Contour plots of the mean thrust coefficient and efficiency for the flexible and rigid foils are shown for the low St range with angle of attack, α, correction in Figure 14 and 15. The contours of C_T for different foils are very comparable; however, as noted, these values are generally higher than in the case of simple harmonic motion. With regard to efficiency, the behavior of the $\eta = 0.70$ contour with increasing flexibility is quite similar to the case of simple harmonic motion. This contour is quite wide for the A60 foil, but nonexistent for the rigid foil. The eighty percent contour again only appears for the A60 foil.

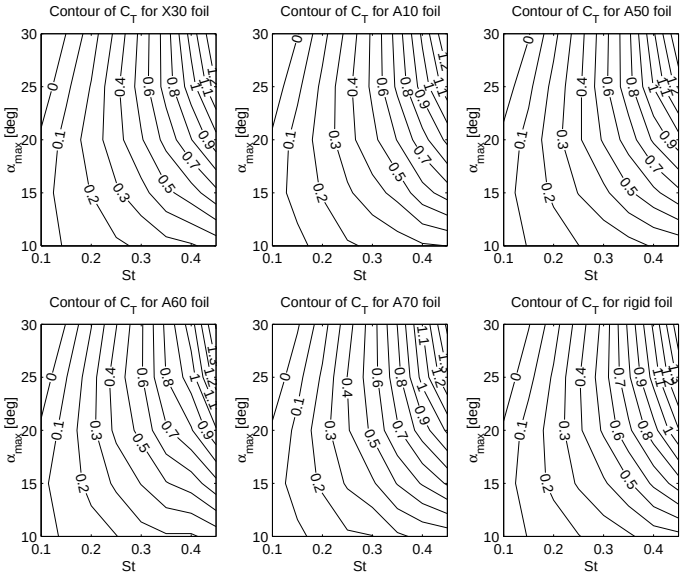

Fig. 14. The contour of the thrust coefficient for Strouhal number between 0.10-0.45

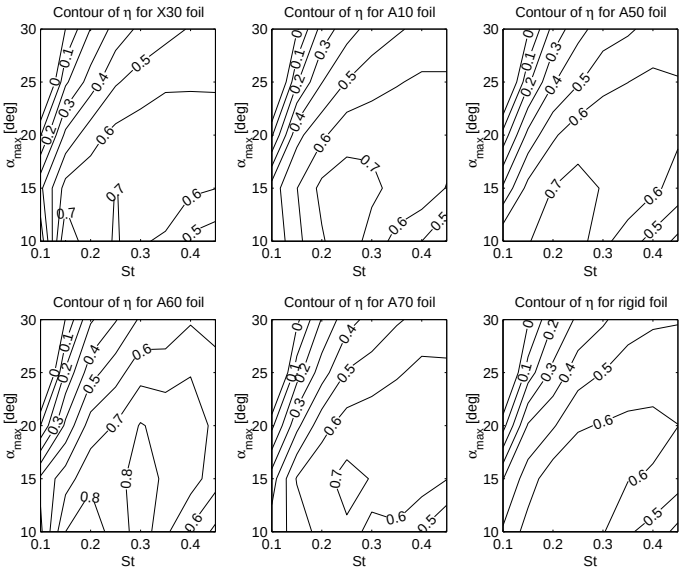

Fig. 15. The contour of the propulsive efficiency for Strouhal number between 0.10-0.45

C. Comparison with propeller propulsion

In evaluating the performance of the flexible foils in comparison to existing propulsors, the rotary propeller is the most suitable reference. First, we need first to redefine the thrust coefficient used up to this point. The thrust coefficient defined for propellers, which we denote by C_{Tp}, uses the swept area of the propeller instead of the wetted area we used for the foils in the C_T calculation. The swept area of the foil is $2h_0s$, and since $h_0 = 0.75c$ for all the tests, we have $C_{Tp} = C_T/1.5$.

There are several types of commonly used propellers; we consider here (a) the Kirsten-Boeing propeller, (b) a contra-rotating propeller set, (c) a pressure disk with ideal efficiency, and (d) the numerical predictions for a propeller using the lift line design tool PLL. The Kirsten-Boeing propeller was originally designed for sport boats and other small vessels. It yields high efficiency in the range of low thrust coefficients. The contra-rotating propeller was initially designed to overcome the instability caused by unbalanced forces on a single propeller, and to partially recover the rotational energy imparted by the propeller to the fluid; later, it emerged as a reliable and high efficiency approach, well suited for larger vessels, such as bulk carriers. Data shown for the Kirsten-Boeing and contrarotating propellers are taken from [3]. Ideal propeller efficiency is based on inviscid flow derivations on an idealized pressure disk, and under the assumption of no rotational losses. The following expression can be derived [3]:

$$\eta_{ideal} = \frac{2}{1 + \sqrt{1 + C_{T_p}}}.$$

This ideal efficiency cannot be reached in practice and hence it is used as a reference for comparison with experimental data on propellers. Lastly, the lifting line theory design code was developed by Coney and Kerwin at MIT, called PLL [6]. The

TABLE IV

The maximum values for the mean C_T and η and normalized C_T and η at different α_{max} and Strouhal number between 0.1 and 0.45 using the harmonic angle of attack profile.

Flexibility	St	α_{max} for $C_{T_{max}}$	$C_{T_{max}}$	$C_{T_{norm}}$	$\tilde{C}_{T_{norm}}$	α_{max} for η_{max}	η_{max}	η_{norm}	$\tilde{\eta}_{norm}$
$ShoreX30$	0.15	15	0.14	1.00	1.00	15	0.64	1.16	1.14
$ShoreA10$		20	0.14	1.00	1.00	15	0.60	1.09	1.07
$ShoreA50$		15	0.14	1.00	1.00	15	0.63	1.15	1.12
$ShoreA60$		15	0.16	1.14	1.14	15	0.66	1.20	1.18
$ShoreA70$		15	0.14	1.00	1.00	15	0.61	1.11	1.09
$Rigid$		20	0.14	1	1.00	15	0.55	1	0.98
$ShoreX30$	0.20	20	0.25	1.04	1.00	15	0.66	0.99	1.03
$ShoreA10$		20	0.24	1.00	0.96	15	0.73	1.10	1.14
$ShoreA50$		20	0.26	1.08	1.04	15	0.70	1.06	1.09
$ShoreA60$		20	0.27	1.13	1.08	15	0.77	1.17	1.20
$ShoreA70$		20	0.26	1.08	1.04	15	0.67	1.01	1.05
$Rigid$		20	0.24	1	0.96	15	0.66	1	1.03
$ShoreX30$	0.25	25	0.38	1.12	1.06	15	0.70	1.04	1.04
$ShoreA10$		25	0.37	1.09	1.03	15	0.74	1.09	1.10
$ShoreA50$		20	0.39	1.15	1.08	15	0.73	1.08	1.09
$ShoreA60$		25	0.45	1.32	1.25	15	0.75	1.10	1.12
$ShoreA70$		25	0.40	1.18	1.11	15	0.73	1.08	1.09
$Rigid$		30	0.34	1	0.94	15	0.68	1	1.01
$ShoreX30$	0.30	25	0.54	0.98	0.96	15	0.68	1.07	1.01
$ShoreA10$		25	0.52	0.95	0.93	15	0.73	1.15	1.08
$ShoreA50$		25	0.57	1.04	1.02	15	0.69	1.09	1.03
$ShoreA60$		25	0.59	1.07	1.05	15	**0.87**	**1.36**	**1.29**
$ShoreA70$		25	0.56	1.02	1.00	15	0.70	1.09	1.04
$Rigid$		25	0.55	1	0.98	15	0.64	1	0.96
$ShoreX30$	0.35	30	0.75	0.91	1.00	15	0.69	1.11	1.05
$ShoreA10$		25	0.74	0.90	0.99	20	0.68	1.09	1.03
$ShoreA50$		30	0.78	0.95	1.04	15	0.68	1.10	1.03
$ShoreA60$		30	0.83	1.01	1.11	15	0.78	1.25	1.18
$ShoreA70$		30	0.80	0.98	1.06	15	0.70	1.13	1.06
$Rigid$		30	0.82	1	1.09	20	0.62	1	0.94
$ShoreX30$	0.40	30	1.04	0.93	1.03	20	0.65	1.05	1.05
$ShoreA10$		30	1.02	0.91	1.01	20	0.67	1.09	1.08
$ShoreA50$		30	1.08	0.96	1.07	20	0.67	1.08	1.08
$ShoreA60$		30	1.05	0.94	1.04	20	0.77	1.24	1.24
$ShoreA70$		30	1.10	0.98	1.09	20	0.69	1.12	1.11
$Rigid$		30	1.12	1	1.11	20	0.62	1	1.00
$ShoreX30$	0.45	30	1.30	0.88	1.01	20	0.63	1.05	1.03
$ShoreA10$		30	1.30	0.88	1.01	20	0.64	1.07	1.05
$ShoreA50$		30	1.39	0.95	1.08	20	0.61	1.02	1.00
$ShoreA60$		30	1.41	0.96	1.09	20	0.67	1.12	1.10
$ShoreA70$		30	1.42	0.97	1.10	20	0.65	1.08	1.07
$Rigid$		30	1.47	1	1.14	20	0.60	1	0.98

PLL predictions we show are obtained from runs made by Haugsdal [7].

As seen in Figure 16 and 17, the results of all foils cluster into clearer groups, when sorted by Strouhal number. The high and low ranges of C_{T_p} denoted give the operational range of high-speed vessels and tankers, respectively.

With increasing angle of attack, the propulsive efficiency decreases while the thrust coefficient increases. The performance gain due to flexibility, primarily in efficiency, is clear for various angles of attack. Both Shore A60 and rigid foils reach the maximum efficiency around Strouhal number of 0.2. With the Strouhal number less than 0.45, gains in efficiency due to the chordwise flexibility are considerable.

The cases of highest performance warrant further discussion; for the A60 foil in particular. Considering the case of harmonic angle of attack profile, $St = 0.30$, and $\alpha_{max} = 15°$, we plot the time traces of linear and rotary motion, lift force, thrust force, and moment, for both the rigid and the A60 foil in Figures 18 and 19. We see that while the thrust and torque are virtually unchanged by the flexibility, the peaks in lift are substantially reduced in the A60 foil. These lift peaks normally occur at the phase of maximum transverse velocity, and hence comprise a large power expense. By reducing the lift peaks, the A60 foil achieves very high efficiency for a given thrust level.

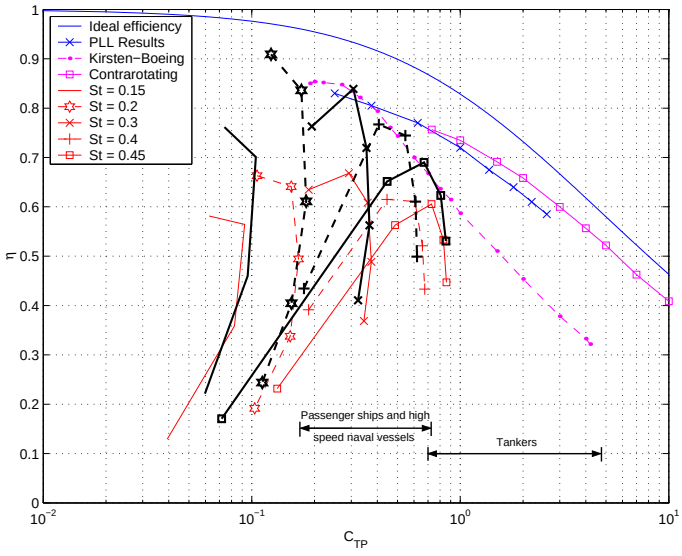

Fig. 16. The propulsive efficiency as function of the C_{T_p}, using simple harmonic motion profile, for different Strouhal number. The thick and thin lines represent the results from Shore A60 and rigid foil, respectively.

V. Summary and Conclusion

Chordwise flexibility in flapping foils, if properly selected, is shown experimentally to improve efficiency with a small decrease in thrust coefficient.

The experiments were conducted with two different kinematic modes of motion; the first uses simple harmonic heave and pitch motion, while the second mode uses a combination

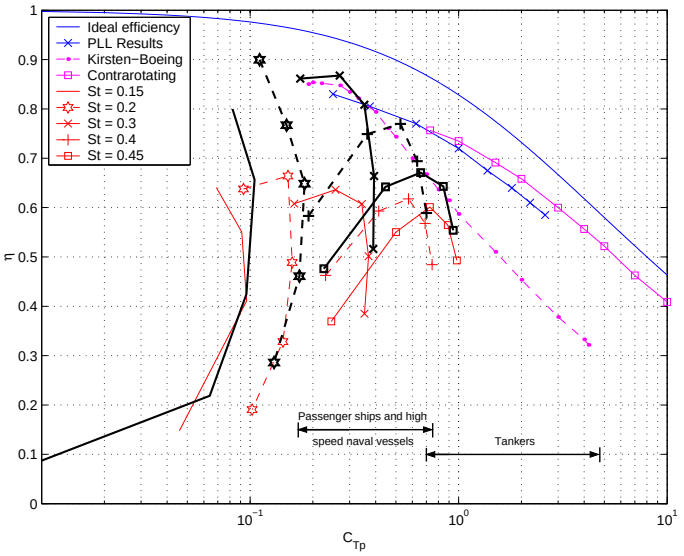

Fig. 17. The propulsive efficiency as function of the C_{T_p}, using harmonic angle of attack profile, for different Strouhal numbers. The thick and thin lines represent the results from Shore A60 and rigid foil, respectively.

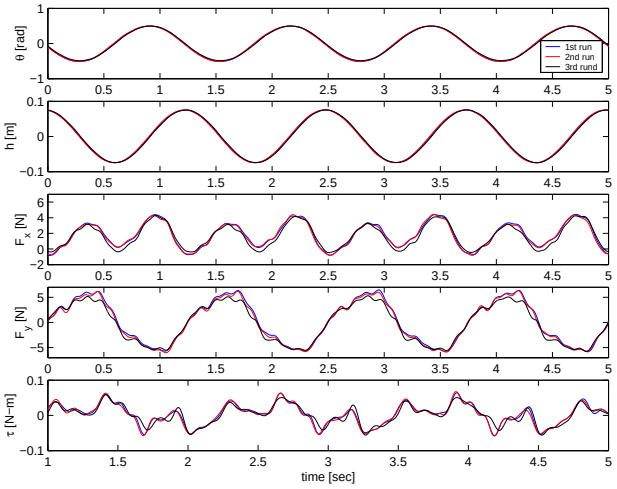

Fig. 18. The time traces of pitch and heave positions, instantaneous thrust and lift forces, and applied torque for the rigid foil, with the simple harmonic motion profile, when St = 0.3 and α = 15°.

of multi-harmonic heave and simple harmonic pitch motion that induces a simple harmonic angle of attack variation. Both modes can cause the efficiency to improve significantly at Strouhal numbers below 0.450 and with properly selected flexibility; up to 36% relative to the rigid foil. The second mode is shown to increase the thrust coefficient substantially for large Strouhal numbers.

In order to provide a scaling law for the effects of flexibility, a non-dimensional flexibility parameter was defined, which expresses the ratio of the elastic force to the hydrodynamic lift force.

Overall, flexible foils can be very efficient propulsors, and are shown to be competitive against rotary propellers.

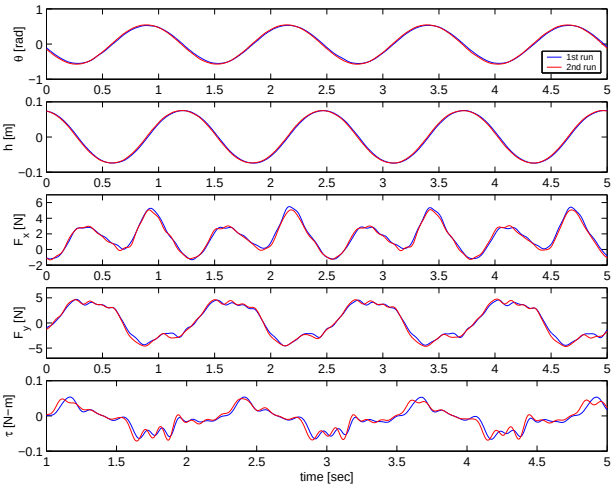

Fig. 19. The time traces of pitch and heave positions, instantaneous thrust and lift forces, and applied torque for the Shore A60 foil, with the harmonic angle of attack profile, when St = 0.3 and α = 15°.

ACKNOWLEDGMENT

Support by NAVSEA, the Office of Naval Research (Drs. T. McMullen and P. Bandyopadhyay) and by the the MIT Sea Grant Program is gratefully acknowledged.

REFERENCES

[1] J.M. Anderson, K. Streitlien, D.S. Barrett and M.S. Triantafyllou, *Oscillating foils of high propulsive efficiency*, J. of Fluid Mech., Vol. 360, pp.41-72, 1998.

[2] N. Bose, *Performance Of Chordwise Flexible Oscillating Propulsors Using A Time-Domain Panel Method* , Int. Shipbuild. Progr., Vol. 42, No. 432, pp. 281-294, 1995.

[3] J.P. Breslin and P. Andersen, *Hydrodynamics of Ship Propellers*, Cambridge ocean technology series; 3, Cambridge University Press, 1994.

[4] M.E. Castelo, *Propulsive Performance of Flexible-Chord Foils* , Bachelor of Science Thesis, Department of Ocean Engineering, MIT, June 2002.

[5] M.G. Chopra, *Large amplitude lunate-tail theory of fish locomotion* , J. of Fluid Mech., Vol. 74, pp.161-182, 1976.

[6] W.B. Coney, *A method for the design of a class of optimum marine propulsors* , Phd Thesis, Department of Ocean Engineering, MIT, 1989.

[7] Ø. Haugsdal, *Motion Control of Oscillating Foils for Steady Propulsion and Starting Maneuvers* , Master of Science Thesis, Department of Ocean Engineering, MIT, June 2000.

[8] S.F. Hoerner, *Fluid-Dynamic Drag* , Hoerner Fluid Dynamics, Vancouver, Washington, 1965.

[9] F.S. Hover, Ø. Haugsdal and M.S. Triantafyllou, *"Control of angle of attack profiles in flapping foil propulsion."*, Journal of Fluids and Structures, accepted 2003.

[10] J. Katz and D. Weihs, *Hydrodynamic propulsion by large amplitude oscillation of an airfoil with chordwise flexibility* , J. Fluid Mech., Vol. 88, pp.485-497, 1978.

[11] J. Katz and D. Weihs, *Large amplitude unsteady motion of a flexible slender propulsor* , J. Fluid Mech., Vol. 90, pp.713-723, 1979.

[12] T. Kudo, A. Kubota, H. Kato and H. Yamaguchi, *Study on Propulsion by Partially Elastic Oscillating Foil (1st and 2nd Reports)* , Journal of Naval Architects of Japan, No. 156, pp.82-101, 1985.

[13] P.S.K. Lai, R.C. McGregor and N. Bose, *Experimental Investigation of oscillating foil propellers* , 22nd American Towing Tank Conference, ATTC conference, St. Johns, August 1989.

[14] M.J. Lighthill, *Aquatic animal propulsion of high hydromechanical efficiency* , J. Fluid Mech., Vol. 44, pp.265-301, 1970.

[15] P. Liu, N. Bose, *Propulsive Performance from Oscillating Propulsors with Spanwise Flexibility* , Proceedings of the Royal Society of London, Vol. 453, Issue 1963, pp. 1763-1770, August 1997.

[16] R. Ramamurti, W.C. Sandberg, R. Lhner, J.A. Walker, *Fluid dynamics of flapping aquatic flight in the bird wrasse: three-dimensional unsteady computations with fin deformation* , The Jouranal of Experimental Biology, Vol. 205, pp.2997-3008, 2002.

[17] D.A. Read, F.S. Hover, M.S. Triantafyllou, *Forces on oscillating foils for propulsion and maneuvering* , J. of Fluids and Structures, Vol. 17, pp.163-183, 2003.

[18] H. Yamaguchi, N. Bose, *Oscillating Foils for Marine Propulsion*, Proceedings of the Fourth International Offshore and Polar Engineering Conference, Vol. 3, pp.539-544, 1994.

[19] I. Yamamoto, Y. Terada, T. Nagamatu, and Y. Imaizumi, *Propulsion System with Flexible/Rigid Oscillating Fin* , IEEE Journal of Ocean Engineering, Vol. 20, No. 1, January 1995.

[20] I. Yamamoto and Y. Terada, *Research On Flexible Oscillating Fin Propulsion System And Robotic Fish* , Second International Symposium on Aqua Bio-Mechanisms, September 2001.

[21] T.Y.-T. Wu, *Hydromechanics of swimming propulsion. Part 1. Swimming of a two-dimensional flexible plate at variable forward speeds in an inviscid fluid* , J. Fluid Mech., Vol. 46, pp. 337-355, 1971.

[22] T.Y.-T. Wu, *Hydromechanics of swimming propulsion. Part 2. Some optimum shape problems* , J. Fluid Mech., Vol. 46, pp. 521-544, 1971.